GaN-Based Optoelectronic Impact Force Sensor

RUAN Junhui, JIANG Chengxiang, XU Shengli, WANG Yongjin, SHI Fan

(GaN Optoelectronic Integration International Cooperation Joint Laboratory of Jiangsu Province, Nanjing University of Posts and Telecommunications, Nanjing 210003, China)

DOI: 10.12142/ZTECOM.202502010

https://kns.cnki.net/kcms/detail/34.1294.TN.20250520.1401.005.html, published online May 20, 2025

Manuscript received: 2024-10-20

Abstract: A monolithic integration of the light emitting diode (LED) and photodetector (PD) based on III-nitride is designed and fabricated on a sapphire substrate to act as a transceiver. Due to the coexistence of light emission and detection phenomenon of the multi-quantum well (MQW) structure, the monolithic transceiver can effectively sense environmental changes. By integrating a deformable Polydimethylsiloxane (PDMS) film on the transceiver chip, external force variation can be effectively detected. As the thickness of the PDMS reduces, the sensitivity significantly improves but at the expense of the measuring range. A sensitivity of 2.968 3% per newton for a range of 0–11 N is obtained when a 2 mm-thick PDMS film is packaged. The proposed monolithic GaN transceiver-based sensing system has the advantages of compactness, low cost, and simple assembly, providing an optional method for practical applications.

Keywords: monolithic integration; III-nitride; transceiver

Citation (Format 1): RUAN J H, JIANG C X, XU S L, et al. GaN-based optoelectronic impact force sensor [J]. ZTE Communications, 2025, 23 (2): 96 – 102. DOI: 10.12142/ZTECOM.202502010

Citation (Format 2): J. H. Ruan, C. X. Jiang, S. L. Xu. et al., "GaN-based optoelectronic impact force sensor," *ZTE Communications*, vol. 23, no. 2, pp. 96 – 102, Jun. 2025. doi: 10.12142/ZTECOM.202502010.

1 Introduction

Miniaturized force sensors have attracted a lot of attention in structural health monitoring[1 – 2], human motion measurement[3], and rail transit monitoring[4]. To date, different kinds of force sensors have been reported such as piezoelectricity, capacitance, and optics[5 – 9]. Compared with electric-based methods, optical sensors have advantages in immunity to electromagnetic interference, fast response and high stability. In terms of optical means, using all-fiber structures as the sensing unit is the most popular strategy. A variety of fiber sensing structures have been developed for force sensing including Mach-Zehnder interferometer[10 – 12], fiber Bragg grating[13 – 14], Fabry-Perot interferometer[15 – 16], etc. Although the wavelength interrogation-based sensing mechanism has the merits of high sensitivity, fast response, and high stability, the system is usually composed of a light source and a spectrometer, which is bulky and complicated to assemble. To miniaturize the system configuration, the integration of the light source, sensing unit and the detector is highly desired.

Recently, GaN and its alloy have been widely used in illumination[17], power electronics[18], display[19], and optical communications[20 – 22] because of their long lifespan, fast response and good optoelectronic properties. Thanks to the ability of light emission and detection of the multi-quantum well (MQW) diode, many GaN-based monolithic devices have been proposed and demonstrated for angle, humidity, pressure, and liquid concentration measurement[23 – 26]. To measure the pressure, microdome-patterned polydimethylsiloxane (PDMS) film and sponges are normally used as the reflection boundary to modulate the reflected light[27 – 29]. However, the common problem facing these microstructure-based PDMS sensing units is that the preparation is relatively complex, and it is difficult to accurately control the shape and distribution of the microstructures.

In this work, a compact design of a GaN optoelectric chip with an Al reflection layer coated PDMS structure for force sensing is proposed. The chip-scale GaN device is composed of a light emitting diode (LED) and a photodetector (PD), which are monolithically integrated on a single wafer, acting as the light emitter and the detector, respectively. The Al-coated PDMS sensing unit is packaged with a gap of 2 mm to the chip. When a force is applied to the surface of the PDMS

This work was supported by the National Key Research and Development Program under Grant No. 2024YFE0204700, Natural Science Foundation of Jiangsu Province under Grant No. BG2024023, and Higher Education Discipline Innovation Project under Grant No. D17018.

structure, the distance between the Al reflection film and the GaN chip changes, which in turn alters the amount of reflected light from the Al film and, consequently, the light received by the PD changes. In this way, the impact force can be effectively detected.

2 GaN-Based Device Design and Fabrication

The schematic diagram of the force sensor is presented in Fig. 1a, which integrates a GaN device with an Al-coated PDMS film. The manufacturing process of the sensing device begins with the mold pouring, using 3D printing to fabricate the molds with controllable thicknesses. The PDMS gel is prepared by mixing the prepolymer and curing agent in a 10:1 ratio, followed by a vacuum processing to eliminate air bubbles. Then the mixture is poured into the printed molds and placed into a heating furnace for 40 min with a curing temperature of 80 °C. After curing, the PDMS film is peeled off from the molds and then attached with a piece of Al reflection membrane in the center. The GaN device is fabricated on a 4-inch GaN wafer, which consists of c-plane sapphire substrates, 3.5 μm thick undoped GaN, 2.2 μm thick Si-doped GaN (n-GaN), 400 nm thick MQW and 0.25 μm thick Mg-doped GaN (p-GaN) from the bottom to the top. To fabricate the GaN device, a 230 nm thick transparent indium tin oxide (ITO) current spreading layer is deposited over p-GaN as a p-contact layer. Two circular regions of a diameter of 210 μm are defined as the active regions of LED and PD by photolithography, and the unmasked areas are etched to the n-GaN surface by inductively coupled plasma (ICP) etching. Subsequently, a deep etching to the sapphire substrate is then performed to realize the device isolation between LED and PD. A 1 μm thick SiO_2 is deposited to form the electrical isolation, and then a window is opened, followed by the deposition of Ni/Al/Ti/Pt/Ti/Pt/Au/Ti/Pt/Ti metal stacks on the n-GaN and ITO surfaces. The physical encapsulation of the sensor is displayed in Fig. 1b, which consists of an optoelectronic chip fixed on a printed circuit board (PCB) and a PDMS film. A manometer is mounted on a linear moving stage and moves axially towards the sensor. As the impact force increases, a larger PDMS deformation directs more light to the PD, thus establishing a relationship between force and photocurrent.

3 Results and Discussion

The electrical and optical characteristics of the device are measured. The current-voltage (I-V) characteristic curve of the LED is presented in Fig. 2a. The turn-on voltage of the device is about 2.2 V, and the inset graph shows the relationship between the output optical power of the LED and the injection current. As shown in Fig. 2b, without illumination, the produced photocurrent level is from 10^{-11} A to 10^{-9} A. As the current starts at 10 mA, the photocurrent level increases dramatically to the order of 10^{-6} A. Fig. 2c illustrates a linear relationship between the PD's photocurrent response and the LED biased currents. To characterize the MQW diode's transceiver capability, the electroluminescence (EL) spectrum of the LED and the response spectrum (RS) of the photodetector are tested, as shown in Fig. 2d. The overlapping regions near 480 nm confirm that the MQW diode can detect light emitted by another MQW diode of the same structure.

To verify the detection ability of the MQW diode, proximity sensing is performed to estimate the distance-dependent photocurrent response. A piece of Al film is placed in front of the

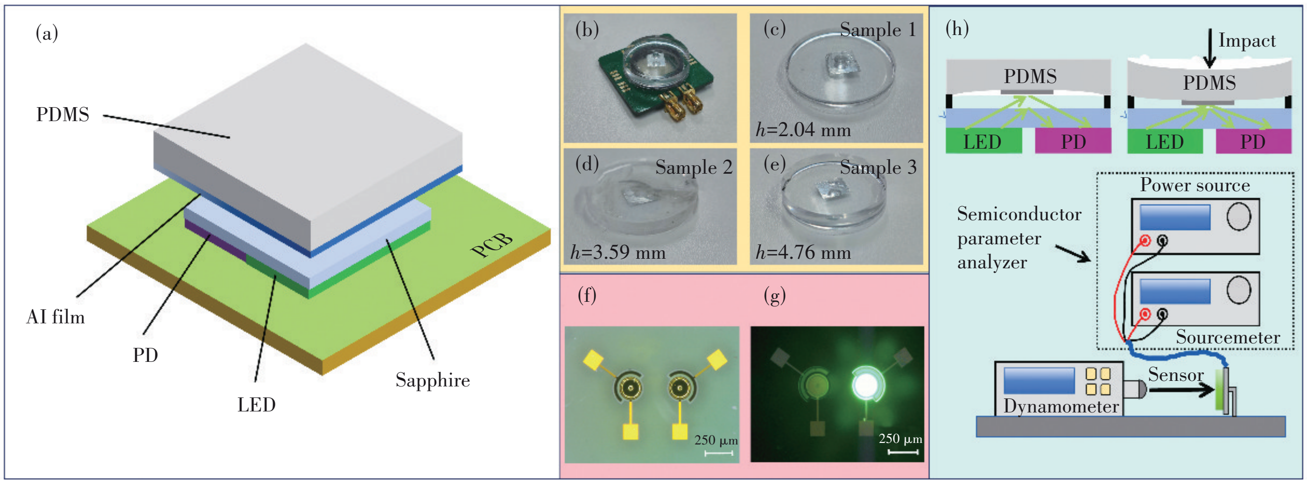

LED: light emitting diode PCB: printed circuit board PD: photodetector PDMS: polydimethylsiloxane

Figure 1. (a) Schematic diagram of the sensor; (b) microphotographs of the physical encapsulation: three kinds of packaged PDMS structures with a thickness of (c) 2.04 mm, (d) 3.59 mm and (e) 4.76 mm, respectively; (f) optical images of the device; (g) LED with biased current at 10 mA; (h) diagram of the experimental setup

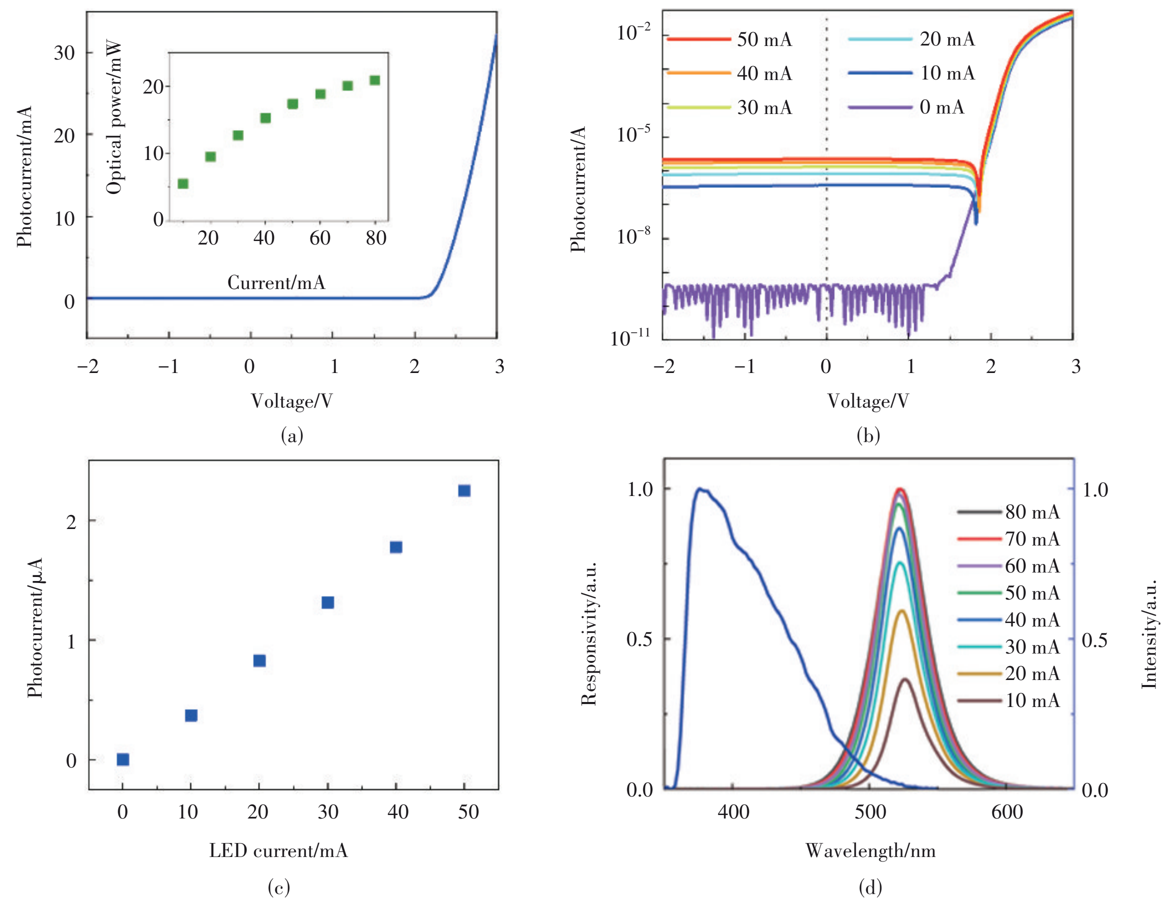

LED: light emitting diode

Figure 2. (a) I-V characteristic of the LED, where the inset shows the output power versus the driven current; (b) I-V curve of PD at different injection currents of LED; (c) Photocurrent response of PD under different currents of LED; (d) RS spectra of PD and the electroluminescence spectra of LED

transceiver chip and moves continuously relative to it. Fig. 3a shows the photocurrent response of the on-chip PD when the distance between the Al film and the transceiver changes from 0 to 12 mm with a step of 2 mm. From the given photocurrent response, it resembles a step-like response curve and exhibits a distinguished detection ability over a wide range, especially at the distance within 2.4 mm. These results suggest that the distance should be optimized around 2 mm to achieve a good sensitivity. Subsequently, the photocurrent response at a spacing distance of 2 mm and a step of 200 μm is studied, as plotted in Fig. 3b, showing a significant change in photocurrent at each step.

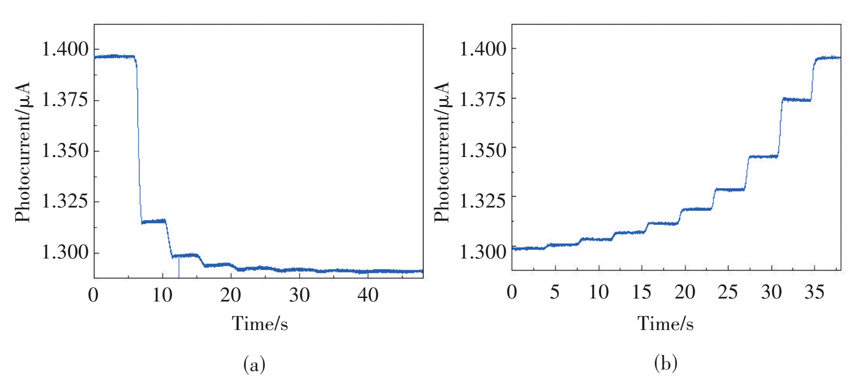

Figure 3. Photocurrent response measured under Al foil moving from (a) 0 to 12 mm, and (b) 0 to 2 mm

In addition to the proximity measurements, a communication performance test of the MQW diode is also carried out to verify the PD's ability to detect transient signal change. The pseudo-random binary sequence (PRBS) data applied to the external light source are generated with a Keysight 33600A series waveform generator. The measured voltages of the PD with a 1 MΩ oscilloscope under incident PRBS data of 100 bit/s, 200 bit/s, 500 bit/s, and 1 000 bit/s are presented in Figs. 4a – 4d, respectively. The received response rate can easily reach 1 000 bit/s without serious signal distortion. The measured fast response rate indicates that the PD can guarantee sufficient resolution for detecting the instantaneous impact signal.

The photocurrent responses of PDMS samples with varying thicknesses under different forces are tested, as illustrated in Fig. 5. The green, blue and red curves represent PDMS with thicknesses of 2.04 mm, 3.59 mm and 4.76 mm, defined as Samples #1, #2, and #3. For Sample #1, it can respond to impact forces in the range of 0 – 11 N, and the instantaneous photocurrent responses at 3.8 N, 7.3 N and 11 N are recorded and plotted. From the given response curves, a better signal-to-noise ratio (SNR) of the photocurrent response is observed at a larger impact force. At a small force of 3.8 N, a jitter of the baseline is observed, which is caused by the limited PDMS deformation, leading to a small varying photocurrent and a small SNR. When the external force increases to 7.3 N and 11 N, as shown in Figs. 5b and 5c, a smooth photocurrent baseline appears and a better photocurrent response can be seen. Similarly, for Sample #2, as depicted in Figs. 5d, 5e, and 5f, the detectable impact force is larger than that of Sample #1, ranging from 12.5 N to 20.5 N, as the sample thickness increases. Sample #3 has a maximum detection ability of 35 N. However, the detection sensitivity is limited due to the relatively thick PDMS.

The stability test for Sample #1 under an 11 N impact force is shown in Fig. 6a. It shows a consistent photocurrent change of approximately 250 nA over 2 000 s, with the photocurrent profile remaining stable throughout the cycle. Fig. 6b depicts the relative photocurrent response to the impact force and the corresponding data for these three samples. The relative photocurrent is defined as $\Delta I/I$, where I is the initial photocurrent and ΔI is the varying photocurrent caused by the impact.

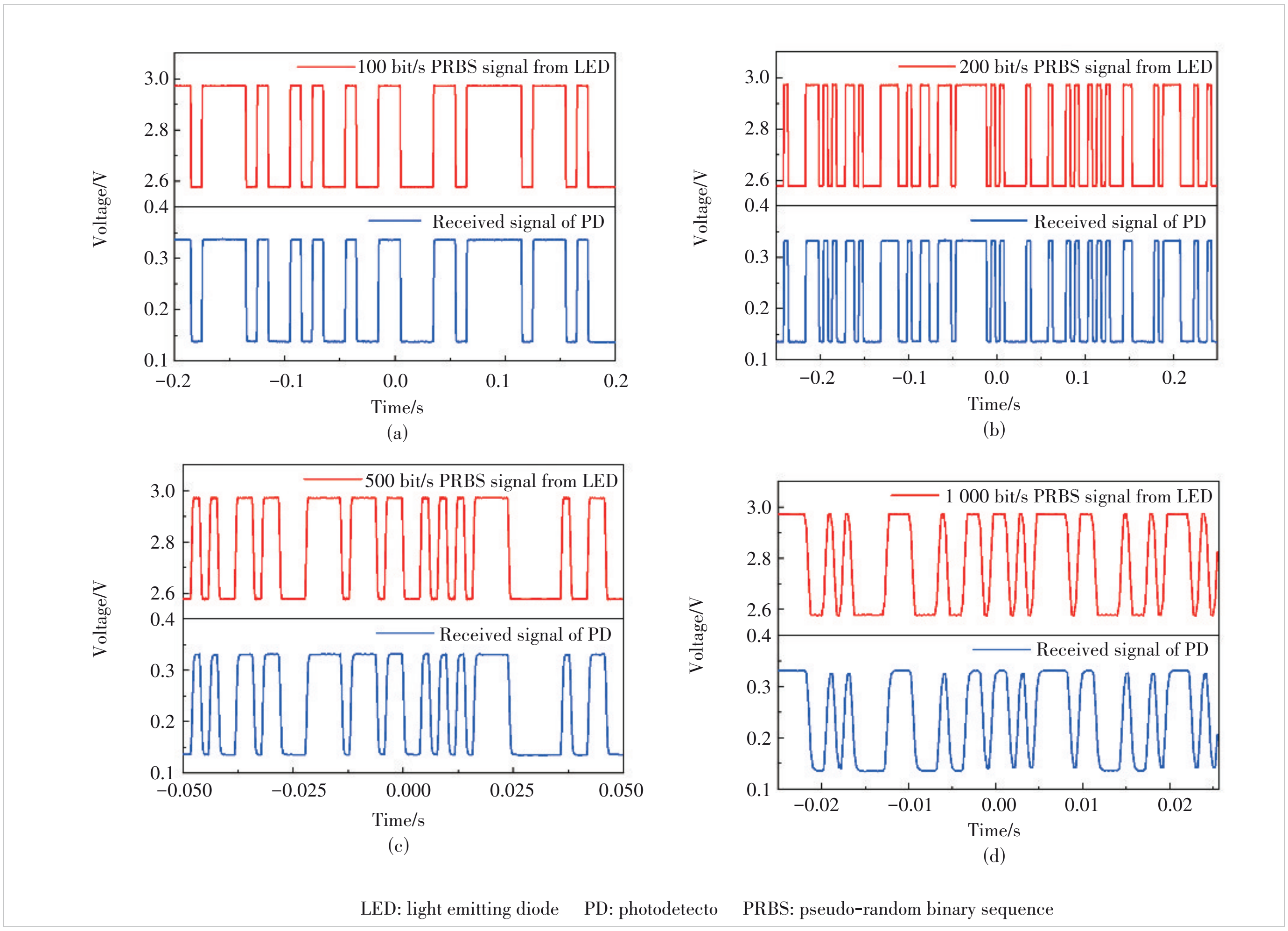

Figure 4. Measured voltages of the PD under incident PRBS data rates of (a) 100 bit/s, (b) 200 bit/s, (c) 500 bit/s, and (d) 1 000 bit/s

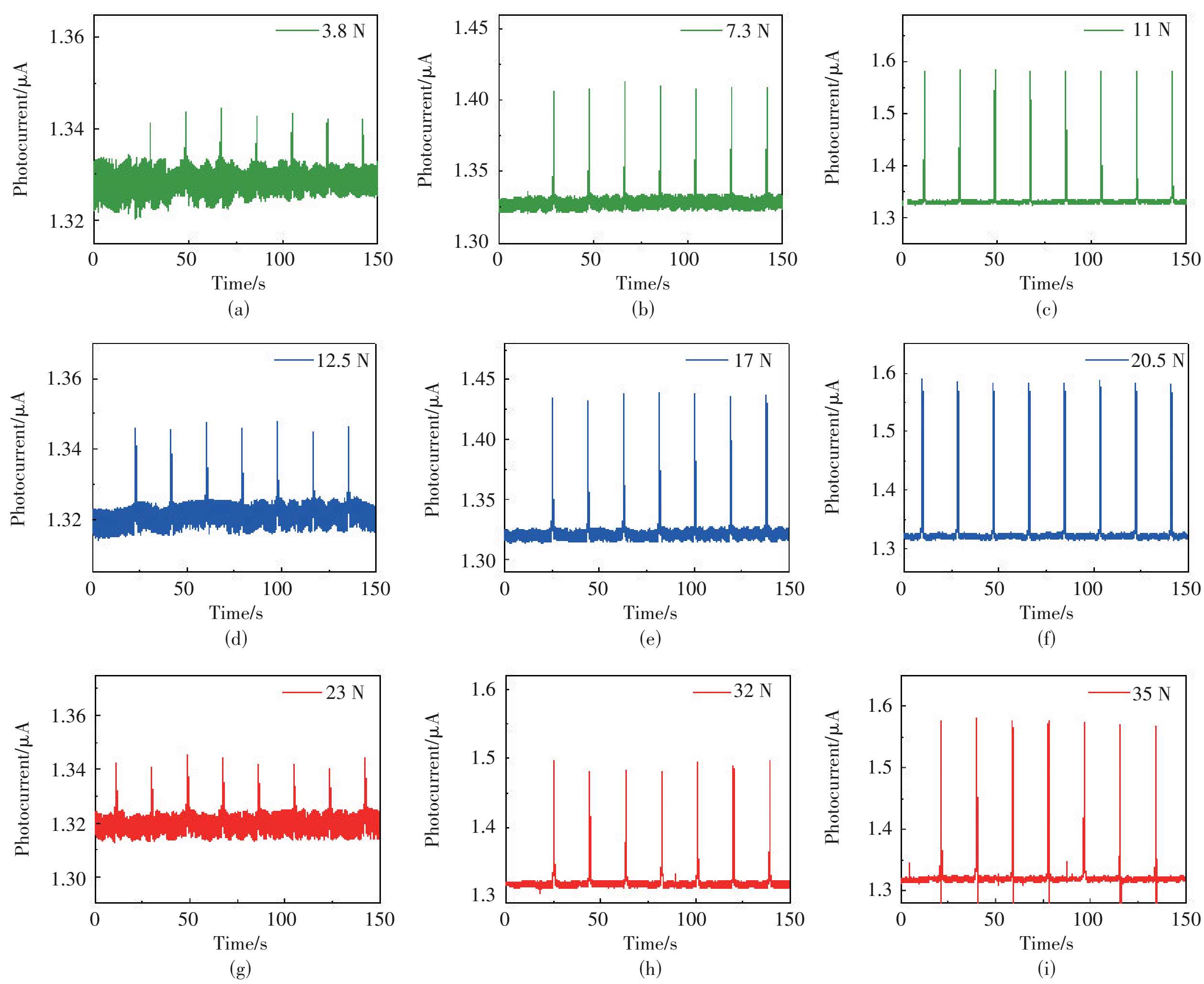

Figure 5. Photocurrent response for Sample #1 under impact forces of (a) 3.8 N, (b) 7.3 N, and (c) 11 N; for Sample #2 under impact forces of (d) 12.5 N, (e) 17 N, and (f) 20.5 N; for Sample #3 under impact forces of (g) 23 N, (h) 32 N, and (i) 35 N

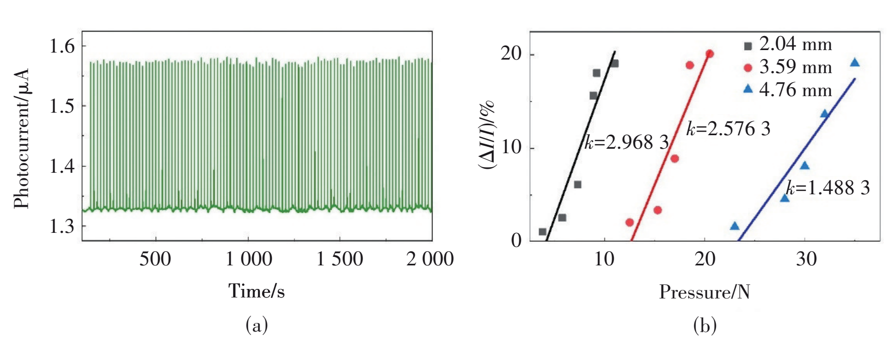

Figure 6. (a) Long-time photocurrent monitor of the sensor with Sample #1; (b) relative photocurrent response of the sensors as functions of impact forces

From the data fitting, Sample #1, the thinnest one, has the highest sensitivity with a slope of 2.968 3% per newton. Sample 2 exhibits a medium sensitivity with a slope of 2.576 3 per newton, while Sample 3, the thickest one, has the lowest sensitivity with a slope of 1.488 3 per newton. Despite the difference in sample thicknesses, the distance between the Al reflector and the chip is set to the same spacing, resulting in the maximum relative photocurrents for all three samples keeping around 20%. The above results reveal that the detection range for impact force can be arbitrarily tailored by selecting PDMS membranes of different thicknesses. In addition, as the thickness of the film increases, the ability to detect the magnitude of the force in-

Table 1. Performance comparison with other force sensors

Method	Linear Range	Sensitivity	Structure Size
Piezoelectric[6]	0.2 – 1.4 N	1.2 V/N	4×4 sensor array (each one: 6×6 mm^2)
Capacitive[7]	0.1 – 1N	0.42 V/N	122×70 mm^2
Capacitive[8]	0.5 – 2 N	N/A	3×0.6×20 mm^3
Capacitive[9]	0 – 9 N	2.8% per newton	22×22×2 mm^3
Fabry-Perot interferometer[15]	0 – 215.4 μN	0.221 pm/μN	20 – 40 mm
Optoelectronic[29]	0 – 40 kPa	0.2 kPa^{-1}	50×50 mm^2
Current work	0 – 35 N	2.96% per newton	2.7×1.8×0.2 mm^3

creases, but the sensitivity decreases. The performance comparisons with other force sensors are summarized in Table 1. The detection range and sensitivity of our current method are comparable to those of piezoelectric and capacitive-based sensors. Notably, the monolithic integration design of our proposed force sensor not only reduces its size to the millimeter scale but also offers advantages in large-scale production and high-density deployment.

4 Conclusions

In summary, a miniature GaN-based impact force sensor is proposed and demonstrated. With a piece of Al attached PDMS film as the force-sensitive unit, deformation of the PDMS induced by the external impact is transformed into the photocurrent changes produced by the transceiver chip. Three PDMS films with different thicknesses are packaged with the transceiver chip to construct impact sensors, and their sensing performances are thoroughly studied. The thickness of PDMS greatly influences the force sensitivity and measurable range. A thin PDMS film is ideal for a low-force and high-sensitivity testing requirement, while a thicker one is better suited for a larger force measurement.

References

[1] CHENG M, ZHU G T, ZHANG F, et al. A review of flexible force sensors for human health monitoring [J]. Journal of advanced research, 2020, 26: 53 – 68. DOI: 10.1016/j.jare.2020.07.001
[2] KENRY, YEO J C, LIM C T. Emerging flexible and wearable physical sensing platforms for healthcare and biomedical applications [J]. Microsystems and nanoengineering, 2016, 2: 16043. DOI: 10.1038/micronano.2016.43
[3] PHAM T H, CARON S, KHEDDAR A. Multicontact interaction force sensing from whole-body motion capture [J]. IEEE transactions on industrial informatics, 2018, 14(6): 2343 – 2352
[4] GAO L, ZHOU C Y, XIAO H, et al. Continuous vertical wheel-rail force reconstruction method based on the distributed Acoustic sensing technology [J]. Measurement, 2022, 197: 111297. DOI: 10.1016/j.measurement.2022.111297
[5] CURRY E J, KE K, CHORSI M T, et al. Biodegradable piezoelectric force sensor [J]. Proceedings of the national academy of sciences of the United States of America, 2018, 115(5): 909 – 914. DOI: 10.1073/pnas.1710874115
[6] EMAMIAN S, NARAKATHU B B, CHLAIHAWI A A, et al. Screen printing of flexible piezoelectric based device on polyethylene terephthalate (PET) and paper for touch and force sensing applications [J]. Sensors and actuators A: physical, 2017, 263: 639 – 647. DOI: 10.1016/j.sna.2017.07.045
[7] GAO S, ARCOS V, NATHAN A. Piezoelectric vs. capacitive based force sensing in capacitive touch panels [J]. IEEE access, 2016, 4: 3769 – 3774
[8] KIM K, PARK J, SUH J H, et al. 3D printing of multiaxial force sensors using carbon nanotube (CNT)/thermoplastic polyurethane (TPU) filaments [J]. Sensors and actuators A: physical, 2017, 263: 493 – 500. DOI: 10.1016/j.sna.2017.07.020
[9] ZHU Y L, CHEN X, CHU K M, et al. Carbon black/PDMS based flexible capacitive tactile sensor for multi-directional force sensing [J]. Sensors, 2022, 22(2): 628. DOI: 10.3390/s22020628
[10] SU H, IORDACHITA I I, TOKUDA J, et al. Fiber optic force sensors for MRI-guided interventions and rehabilitation: a review [J]. IEEE sensors journal, 2017, 17(7): 1952 – 1963. DOI: 10.1109/JSEN.2017.2654489
[11] YUAN W H, YANG Z R, CUI M J, et al. A ring core fiber sensor based on Mach-Zehnder interferometer for transversal force sensing with solvable temperature cross sensitivity [J]. IEEE sensors journal, 2023, 23(4): 3615 – 3622. DOI: 10.1109/JSEN.2023.3234906
[12] LEE C W, LEE J H, SEOK H. Squeezed-light-driven force detection with an optomechanical cavity in a Mach-Zehnder interferometer [J]. Scientific reports, 2020, 10: 17496. DOI: 10.1038/s41598-020-74629-1
[13] XIONG L, JIANG G Z, GUO Y X, et al. A three-dimensional fiber Bragg grating force sensor for robot [J]. IEEE sensors journal, 2018, 18 (9): 3632 – 3639. DOI: 10.1109/JSEN.2018.2812820
[14] LAI W J, CAO L, LIU J J, et al. A three-axial force sensor based on fiber Bragg gratings for surgical robots [J]. IEEE/ASME transactions on mechatronics, 2022, 27(2): 777 – 789. DOI: 10.1109/TMECH.2021.3071437
[15] GONG Y, YU C B, WANG T T, et al. Highly sensitive force sensor based on optical microfiber asymmetrical Fabry-Perot interferometer [J]. Optics express, 2014, 22(3): 3578 – 3584. DOI: 10.1364/OE.22.003578
[16] DASH J N, LIU Z Y, GUNAWARDENA D S, et al. Fabry-Perot cavity-based contact force sensor with high precision and a broad operational range [J]. Optics letters, 2019, 44(14): 3546 – 3549. DOI: 10.1364/OL.44.003546
[17] XIE E Y, CHEN C, OUYANG C S, et al. GaN-based series hybrid LED array: a dual-function light source with illumination and high-speed visible light communication capabilities [J]. Journal of lightwave technology, 2024, 42(1): 243 – 250. DOI: 10.1109/JLT.2023.3303779
[18] FLACK T J, PUSHPAKARAN B N, BAYNE S B. GaN technology for power electronic applications: a review [J]. Journal of electronic materials, 2016, 45(6): 2673 – 2682. DOI: 10.1007/s11664-016-4435-3
[19] ZHU S J, SHAN X Y, LIN R Z, et al. Characteristics of GaN-on-Si green micro-LED for wide color gamut display and high-speed visible light communication [J]. ACS photonics, 2023, 10(1): 92 – 100. DOI: 10.1021/acsphotonics.2c01028
[20] CHANG Y H, HUANG Y M, LIOU F J, et al. 2.805 Gbit/s high-bandwidth phosphor white light visible light communication utilizing an InGaN/GaN semipolar blue micro-LED [J]. Optics express, 2022, 30(10): 16938 – 16946. DOI: 10.1364/OE.455312
[21] YU H B, MEMON M H, WANG D H, et al. AlGaN-based deep ultraviolet micro-LED emitting at 275 nm [J]. Optics letters, 2021, 46(13): 3271 – 3274. DOI: 10.1364/OL.431933
[22] MEMON M H, YU H B, LUO Y M, et al. A three-terminal light emitting and detecting diode [J]. Nature electronics, 2024, 7(4): 279 – 287. DOI: 10.1038/s41928-024-01142-y
[23] YIN J H, YANG H Y, LUO Y M, et al. III-nitride microsensors for 360° angle detection [J]. IEEE electron device letters, 2022, 43(3): 458 – 461. DOI: 10.1109/LED.2022.3148232
[24] YU B L, LUO Y M, CHEN L, et al. An optical humidity sensor: a compact photonic chip integrated with artificial opal [J]. Sensors and actuators B: chemical, 2021, 349: 130763. DOI: 10.1016/j.snb.2021.130763

[25] YU B L, LUO Y M, LI J, et al. Interface engineering in chip-scale GaN optical devices for near-hysteresis-free hydraulic pressure sensing [J]. ACS applied materials & interfaces, 2022, 14(33): 38351 – 38357. DOI: 10.1021/acsami.2c09291

[26] QIN F F, LU X Y, CHEN Y, et al. Concentration sensing system with monolithic InGaN/GaN photonic chips [J]. Chinese optics letters, 2024, 22(6): 062501. DOI: 10.3788/col202422.062501

[27] AN X S, LUO Y M, YU B L, et al. A chip-scale GaN-based optical pressure sensor with microdome-patterned polydimethylsiloxane (PDMS) [J]. IEEE electron device letters, 2021, 42(10): 1532 – 1535. DOI: 10.1109/LED.2021.3103891

[28] ZHAN J, ZHU L, HE Z, et al. Impact force sensors based on GaN optical devices with micropatterned PDMS sponges [J]. IEEE sensors journal, 2023, 23(17): 19226 – 19231. DOI: 10.1109/JSEN.2023.3295931

[29] RAMUZ M, TEE B C, TOK J B, et al. Transparent, optical, pressure-sensitive artificial skin for large-area stretchable electronics [J]. Advanced materials (Deerfield Beach, Fla.), 2012, 24(24): 3223 – 3227

Biographies

RUAN Junhui is currently pursuing his bachelor's degree at the School of Communications and Information Engineering, Nanjing University of Posts and Telecommunications, China. His research interests include optical fiber sensing, GaN optoelectronics sensors, and analog circuit design.

JIANG Chengxiang is currently pursuing his master's degree at the School of Communications and Information Engineering, Nanjing University of Posts and Teleommunications, China. His research interests include GaN devices and visible light communications.

XU Shengli is currently pursuing his bachelor's degree at the School of Communications and Information Engineering, Nanjing University of Posts and Teleommunications, China. His research interests focus on digital signal processing and hardware circuit design.

WANG Yongjin received his PhD degree in microelectronics and solid-state electronics from Shanghai Institute of Microsystem and Information Technology, Chinese Academy of Sciences, China in 2005. He was engaged in the research work with the University of Freiburg, Germany, Tohoku University, Japan, Forschungszentrum Jülich, Germany, and the University of Bristol, UK. Since 2011, he has been a professor with the Nanjing University of Posts and Telecommunications, China, where he is currently the chief investigator of National Innovation Base for Micro-Nano Device and Information System. His research interests include III-nitride monolithic photonic circuit for visible light communication and the Internet of Things. He was the recipient of many scholarships, including the Humboldt Foundation Scholarship, the JSPS Special Researcher Scholarship, and the Royal Society for Engineering Scholarship.

SHI Fan (sf123@njupt.edu.cn) received his PhD degree from the School of Communications and Information Engineering, Shanghai University, China in 2020. He has joined the School of Communications and Information Engineering, Nanjing University of Posts and Telecommunications, China as a lecturer since 2020. His research interests include GaN devices, visible light communication, and mode-locked fiber lasers.